LETTERS

Photon blockade in an optical cavity with one trapped atom

K. M. Birnbaum[1], A. Boca[1], R. Miller[1], A. D. Boozer[1], T. E. Northup[1] & H. J. Kimble[1]

At low temperatures, sufficiently small metallic[1] and semiconductor[2] devices exhibit the 'Coulomb blockade' effect, in which charge transport through the device occurs on an electron-by-electron basis[3]. For example, a single electron on a metallic island can block the flow of another electron if the charging energy of the island greatly exceeds the thermal energy. The analogous effect of 'photon blockade' has been proposed for the transport of light through an optical system; this involves photon–photon interactions in a nonlinear optical cavity[4–13]. Here we report observations of photon blockade for the light transmitted by an optical cavity containing one trapped atom, in the regime of strong atom–cavity coupling[14]. Excitation of the atom–cavity system by a first photon blocks the transmission of a second photon, thereby converting an incident poissonian stream of photons into a sub-poissonian, anti-bunched stream. This is confirmed by measurements of the photon statistics of the transmitted field. Our observations of photon blockade represent an advance over traditional nonlinear optics and laser physics, into a regime with dynamical processes involving atoms and photons taken one-by-one.

An analogy between electron transport in mesoscopic electronic devices and photon transport through strongly coupled optical systems was originally suggested in ref. 5. These authors proposed that an effect similar to Coulomb blockade for electrons[1–3] might be possible for photons by using photon–photon interactions in a nonlinear optical cavity[5]. In this scheme, strong dispersive interactions enabled by electromagnetically induced transparency (EIT) cause the presence of a 'first' photon within the cavity to block the transmission of a 'second' photon, leading to an ordered flow of photons in the transmitted field.

After resolution of an initial difficulty[6], subsequent work has confirmed that such photon blockade is indeed feasible for a single intracavity atom by way of a multi-state EIT scheme[7–9]. Photon blockade is possible in other settings, including in concert with Coulomb blockade[10] and via tunnelling with localized surface plasmons[11]. Photon blockade has also been predicted for a two-state atom coupled to a cavity mode[4,9,12,13]. As illustrated in Fig. 1a, the underlying mechanism is the anharmonicity of the Jaynes–Cummings ladder of eigenstates[4,15]. Resonant absorption of a photon of frequency ω_- to reach the state $|1,-\rangle$ (where $|n,+(-)\rangle$ denotes the higher- (lower-) energy eigenstate with n excitations) 'blocks' the absorption of a second photon at ω_- because transitions to $|2,\pm\rangle$ are detuned from resonance.

Whereas electrons interact directly via Coulomb repulsion, photon–photon interactions must be mediated by matter. Furthermore, verification of this effect requires measurements of the quantum statistics of the field; in contrast, Coulomb blockade can be inferred directly from mean transport. Scattering from a single atom in free space, for example, provides a fundamental example of photon blockade[16], albeit with the fluorescent field distributed over 4π and the flux limited by the rate of spontaneous decay γ. In contrast, cavity-mediated schemes offer the possibility of photon emission into a collimated spatial mode with high efficiency and at a rate set by the cavity decay rate κ, which can be much larger than γ. Achieving photon blockade for a single atom in a cavity requires us to operate in the regime of strong coupling, for which the frequency scale g_0 associated with reversible evolution of the atom–cavity system exceeds the dissipative rates (γ, κ) (ref. 14).

Here we report observations of photon blockade in the light transmitted by an optical cavity containing one atom strongly coupled to the cavity field. For coherent excitation at the cavity

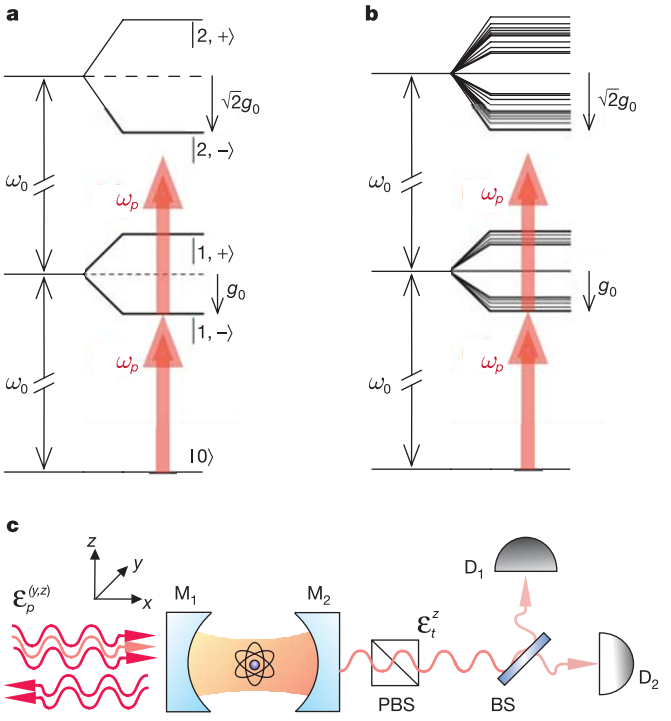

Figure 1 | The atomic level structure used for implementation of the photon blockade effect, and a simple diagram of the experiment. a, Atomic level diagram showing the lowest-energy states for a two-state atom of transition frequency ω_A coupled (with single-photon Rabi frequency g_0) to a mode of the electromagnetic field of frequency ω_C, with $\omega_A = \omega_C \equiv \omega_0$ (ref. 15). Two-photon absorption is suppressed for a probe field ω_p (arrows) tuned to excite the transition $|0\rangle \rightarrow |1,-\rangle$, $\omega_p = \omega_0 - g_0$, leading to $g^{(2)}(0) < 1$ (ref. 13). **b**, Eigenvalue structure for the $(F = 4, m_F) \leftrightarrow (F' = 5', m_F')$ transition coupled to two degenerate cavity modes $l_{y,z}$, as discussed in the Supplementary Information. Two-photon absorption is likewise blocked for excitation tuned to the lowest eigenstate (arrows). **c**, Simple diagram of the experiment. BS, beam splitter.

[1]Norman Bridge Laboratory of Physics 12-33, California Institute of Technology, Pasadena, California 91125, USA.

input, the photon statistics for the cavity output are investigated by measurement of the intensity correlation function $g^{(2)}(\tau)$, which demonstrates the manifestly nonclassical character of the transmitted field. Explicitly, we find $g^{(2)}(0) = (0.13 \pm 0.11) < 1$ with $g^{(2)}(0) < g^{(2)}(\tau)$, so that the output light is both subpoissonian and antibunched[17]. We find that $g^{(2)}(\tau)$ rises to unity at a time $\tau \simeq 45\,\mathrm{ns}$, which is consistent with the lifetime $\tau_- = 2/(\gamma + \kappa) = 48\,\mathrm{ns}$ for the state $|1,-\rangle$ associated with the blockade. Over longer timescales, cavity transmission exhibits modulation arising from the oscillatory motion of the atom trapped within the cavity mode. We use this modulation to make an estimate of the energy distribution for the atomic centre-of-mass motion and infer a maximum energy $E/k_B \approx 250\,\mu K$, where k_B is the Boltzmann constant

The schematic of our experiment in Fig. 1c illustrates the Fabry–Perot cavity formed by mirrors (M_1, M_2) into which single optically cooled caesium atoms are loaded. Atoms are trapped within the cavity by a far-off-resonance trap (FORT), which is created by exciting a TEM_{00} cavity mode at $\lambda_F = 935.6\,\mathrm{nm}$ (ref. 18). To achieve strong coupling, we use the $6S_{1/2}, F = 4 \rightarrow 6P_{3/2}, F' = 5'$ transition of the D2 line in caesium at $\lambda_A = 852.4\,\mathrm{nm}$ (subscript A refers to 'atom'), for which the maximum rate of coherent coupling is $g_0/2\pi = 34\,\mathrm{MHz}$ for $(F = 4, m_F = \pm 4) \rightarrow (F' = 5', m'_F = \pm 5)$. The transverse decay rate for the $6P_{3/2}$ atomic states is $\gamma/2\pi = 2.6\,\mathrm{MHz}$, while the cavity field decays at rate $\kappa/2\pi = 4.1\,\mathrm{MHz}$. The parameters of the cavity are further discussed in the Methods.

A variety of factors make our atom–cavity system more complex than the simple situation described by the Jaynes–Cummings eigenstates, including most significantly that (1) the cavity supports two modes $l_{y,z}$ with orthogonal linear polarizations $(\hat{y}, \hat{z})$ near $\lambda_A = 852.4\,\mathrm{nm}$ as described in the Methods section, and (2) a multiplicity of Zeeman states are individually coupled to these modes for transitions between the manifolds $(F = 4, m_F) \leftrightarrow (F' = 5', m'_F)$. An indication of the potential for this system to achieve photon blockade is provided in Fig. 1b, which displays the actual eigenvalue structure for the first two excited manifolds obtained by direct diagonalization of the interaction hamiltonian, as discussed in the Supplementary Information. As for the basic two-state system, excitation to the lowest-energy state in the one-excitation manifold 'blocks' subsequent excitation because the transitions to the two-excitation manifold are out of resonance.

To substantiate this picture quantitatively, we present in Fig. 2 theoretical results from the steady-state solution to the master equation in various situations, all for the case of coincident atomic and cavity resonances $\omega_A = \omega_{C_1} \equiv \omega_0$. (Subscripts C_1 and C_2 refer to the cavity resonances near λ_A and λ_B, respectively). Beginning with the ideal setting of a two-state atom coupled to a single cavity mode, we display in Fig. 2a results for the probe transmission spectrum $T(\omega_p)$ and the intensity correlation function $g^{(2)}(0)$ of the field ε_t transmitted by mirror M_2 for excitation by a coherent-state probe ε_p of variable frequency ω_p incident upon the cavity mirror M_1. Clearly evident in $T(\omega_p)$ are two peaks at $\omega_p = \omega_\pm \equiv \omega_0 \pm g_0$ associated with the vacuum-Rabi splitting for the states $|1,\pm\rangle$. At these peaks, ε_p is detuned for excitation $|1,\pm\rangle \rightarrow |2,\pm\rangle$, resulting in $g^{(2)}(0) < 1$ for ε_t. The poissonian photon statistics of the incident probe are thereby converted to subpoissonian statistics for the transmitted field by way of the photon blockade effect illustrated in Fig. 1a. For strong coupling in the weak-field limit, $g^{(2)}(0) \propto (\kappa + \gamma)^2/g_0^2$ for $\omega_p = \omega_\pm$ (ref. 12), hence the premium on achieving $g_0 \gg (\kappa, \gamma)$. By contrast, for $\omega_p = \omega_0 \pm g_0/\sqrt{2}, \varepsilon_p$ is resonant with the two-photon transition $|0\rangle \rightarrow |2,\pm\rangle$, resulting in superpoissonian statistics with $g^{(2)}(0) \gg 1$. For $\omega_p = \omega_0$, there is extremely large bunching due to quantum interference between ε_p and the atomic polarization[12,19].

In Fig. 2b we examine the more complex situation relevant to our actual experiment, namely a multi-state atom coupled to two cavity modes with orthogonal polarizations $\hat{y}, \hat{z}$. Most directly related to the simple case of Fig. 2a is to excite one polarization eigenmode with the incident probe, taken here to be ε_p^z, and to detect the transmitted field ε_t^z for this same polarization, with the transmission spectrum and intensity correlation function denoted by $T_{zz}(\omega_p)$, $g_{zz}^{(2)}(0)$, respectively. Even for the full multiplicity of states for the $F = 4 \rightarrow F' = 5'$ transition coupled to the two cavity modes $l_{y,z}$, $T_{zz}(\omega_p)$ displays a rather simple structure, now with a multiplet structure in place of the single vacuum-Rabi peak around $\omega_p \simeq \omega_0 \pm g_0$. For a probe frequency tuned to the eigenvalues $\omega_p = \omega_0 \pm g_0$, $g_{zz}^{(2)}(0) \simeq 0.7$, once again dropping below unity as in Fig. 2a.

An alternative scheme is to detect along $\hat{z}$, but excite along orthogonal polarization $\hat{y}$, with the respective transmission and correlation functions $T_{yz}(\omega_p)$, $g_{yz}^{(2)}(0)$ also shown in Fig. 2b. Similar to $T_{zz}(\omega_p)$, $T_{yz}(\omega_p)$ exhibits a multiplet structure in the vicinity of $\omega_p \simeq \omega_0 \pm g_0$ owing to the nature of the first excited states of the atom–cavity system. At the extremal $\omega_p = \omega_0 \pm g_0$, $g_{yz}^{(2)}(0)$ reaches a value $g_{yz}^{(2)}(0) \simeq 0.03$ much smaller than for either $g^{(2)}(0)$ in Fig. 2a, or $g_{zz}^{(2)}(0)$ in Fig. 2b, for the same values of (g_0, κ, γ). Our preliminary hypothesis is that this reduction relates to the absence of the superposed driving field ε_p^y with the transmitted field ε_t^z of orthogonal polarization $\hat{z}$ (ref. 20); photons in the mode l_z derive from emissions associated with the atomic components of atom-field eigenstates.

Tuning the probe to $\omega_p = \omega_0 \pm g_0$ has the additional benefit of reducing sensitivity to atomic position, which varies experimentally owing to atomic motion and the multiplicity of trapping sites within the cavity[21]. The atomic position affects the transmission via the position dependence of the coupling $g = g_0\psi(\mathbf{r})$, where ψ is the TEM_{00} spatial mode at λ_{C_1} with maximum $|\psi| = 1$, and $\mathbf{r}$ is the position of the atom. $T_{yz}(\omega_p)$ is small when $|\omega_p - \omega_0| \gtrsim g$, so atoms which have a lower-than-expected value of g will have a reduced contribution to the photon statistics.

An important step in the implementation of this strategy is our recent measurement of the vacuum-Rabi spectrum $T_{zz}(\omega_p)$ for one trapped atom[21]. In that work we obtained quantitative agreement on an atom-by-atom basis between our observations and an extension of the theoretical model used to generate the various plots in Fig. 2b. The extended model incorporates a.c.-Stark shifts from the FORT as well as cavity birefringence. This model predicts that corrections to

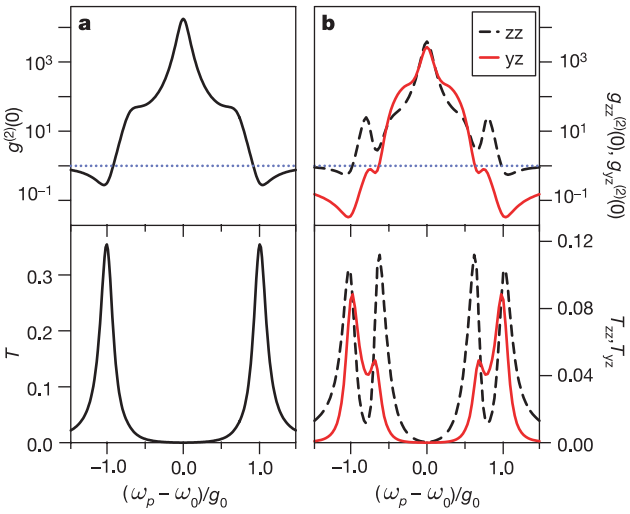

Figure 2 | Theoretical results for the transmission spectra and intensity correlation functions. **a**, $T(\omega_p)$, $g^{(2)}(0)$; **b**, $T_{zz}(\omega_p)$, $g_{zz}^{(2)}(0)$ (dashed) and $T_{yz}(\omega_p)$, $g_{yz}^{(2)}(0)$ (red) from the steady-state solution to the master equation. Included are all transitions $(F = 4, m_F) \leftrightarrow (F' = 5', m'_F)$ with their respective coupling coefficients $g_0^{(m_F, m'_F)}$, as well as the two cavity modes $l_{y,z}$ here assumed to be degenerate in frequency (see Supplementary Information for further discussion). The blue dotted lines indicate poissonian statistics. Parameters are $(g_0, \kappa, \gamma)/2\pi = (33.9, 4.1, 2.6)$ MHz, and the probe strength is such that the intracavity photon number on resonance without an atom is 0.05.

$g^{(2)}_{yz}(0)$ due to these effects are small for our parameters, as discussed in the Supplementary Information.

With these capabilities, we now report measurements of $g^{(2)}_{yz}(\tau)$ for the light transmitted by a cavity containing a single trapped atom. We tune the probe ε^{y}_{p} to $(\omega_p - \omega_0)/2\pi = -34\,\mathrm{MHz}$, near $-g_0$, and acquire photoelectric counting statistics of the field ε^{z}_{t} by way of two avalanche photodiodes (D_1, D_2), as illustrated in Fig. 1c. From the record of these counts, we are able to determine $g^{(2)}_{yz}(\tau)$ by using the procedures discussed in ref. 22. Data are acquired for each trapped atom by cycling through probing, testing, and cooling intervals (of durations $\Delta t_{\mathrm{probe}} = 500\,\mu\mathrm{s}$, $\Delta t_{\mathrm{test}} = 100\,\mu\mathrm{s}$ and $\Delta t_{\mathrm{cool}} = 1.4\,\mathrm{ms}$, respectively) using a procedure similar to that of ref. 21. The test beam is polarized along $\hat{z}$ and resonant with the cavity. A repumping beam transverse to the cavity axis and resonant with $6S_{1/2}$, $F = 3 \rightarrow 6P_{3/2}$, $F' = 4'$ also illuminates the atom during the probe and test intervals. This beam prevents accumulation of population in the $F = 3$ ground state caused by the probe off-resonantly exciting the $F = 4 \rightarrow F' = 4'$ transition. All probing/cooling cycles end after an interval $\Delta t_{\mathrm{tot}} = 0.3\,\mathrm{s}$, at which point a new loading cycle is initiated. We select for the presence of an atom by requiring that $T_{zz}(\omega_p \simeq \omega_{C_1}) \lesssim 0.35$ for the test beam. We use only those data records associated with probing intervals after which the presence of an atom was detected and for which the presence of an atom was detected in all preceding intervals. If there is no atom and the probe is tuned to be resonant with the cavity ($\omega_p = \omega_{C_1}$), then the photon number in mode l_y due to ε^{y}_{p} is 0.21 and the polarizing beam splitter at the output of the cavity (PBS in Fig. 1c) suppresses detection of this light by a factor of ~94.

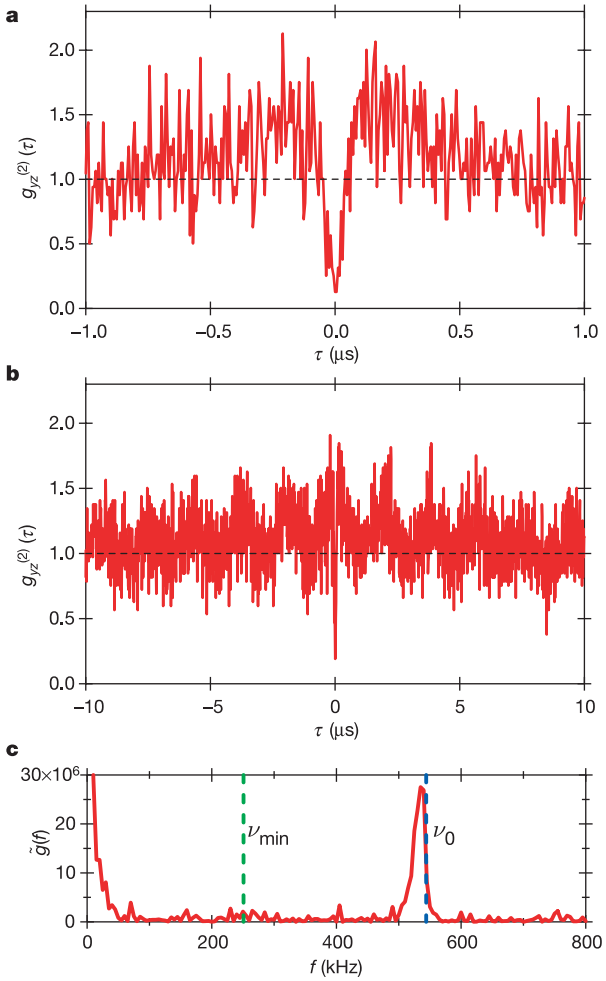

Figure 3 | Experimental measurements of the intensity correlation function $g^{(2)}_{yz}(\tau)$ for incident excitation with polarization along $\hat{y}$ and detection with orthogonal polarization $\hat{x}$. **a**, $g^{(2)}_{yz}(\tau)$ over the interval $|\tau| \leq 1.0\,\mu\mathrm{s}$ demonstrates that the transmitted field exhibits both subpoissonian photon statistics $g^{(2)}_{yz}(0) = (0.13 \pm 0.11) < 1$ and photon antibunching $g^{(2)}_{yz}(0) < g^{(2)}_{yz}(\tau)$ (ref. 17). **b**, $g^{(2)}_{yz}(\tau)$ over longer intervals $|\tau| \leq 10\,\mu\mathrm{s}$ displays a pronounced modulation due to axial motion of the trapped atom. **c**, The Fourier transform $\tilde{g}(f)$ of $g^{(2)}_{yz}(\tau)$ with the independently determined minimum and maximum frequencies ν_{min} and ν_0 for axial motion in a FORT well indicated by the dotted lines. $g^{(2)}_{yz}(\tau)$ is plotted with 6-ns resolution in **a** and with 12-ns resolution in **b**.

Figure 3 presents an example of $g^{(2)}_{yz}(\tau)$ determined from the recorded time-resolved coincidences at (D_1, D_2). In Fig. 3a, the manifestly nonclassical character of the transmitted field is clearly observed with a large reduction in $g^{(2)}_{yz}(0)$ below unity, $g^{(2)}_{yz}(0) = (0.13 \pm 0.11) < 1$, corresponding to the subpoissonian character of the transmitted field, and with $g^{(2)}_{yz}(0) < g^{(2)}_{yz}(\tau)$ as a manifestation of photon antibunching. We find that $g^{(2)}(\tau)$ rises to unity at a time $\tau \simeq 45\,\mathrm{ns}$, which is consistent with a simple estimate of $\tau_- = 2/(\gamma + \kappa) = 48\,\mathrm{ns}$ based upon the lifetime for the state $|1, -\rangle$.

Although for small $|\tau|$ our observations of $g^{(2)}_{yz}(\tau)$ are in reasonable agreement with the predictions from our theoretical model, there are significant deviations on longer timescales. Modulation that is not present in the model is evident in Fig. 3b, which arises from the centre-of-mass motion of the trapped atom. In support of this assertion, Fig. 3c displays the Fourier transform $\tilde{g}(f)$ of $g^{(2)}_{yz}(\tau)$, which exhibits a narrow peak at frequency $f_0 \simeq 535\,\mathrm{kHz}$ just below the independently determined frequency $\nu_0 \simeq 544\,\mathrm{kHz}$ for harmonic motion of a trapped atom about an antinode of the FORT in the axial direction x. This modulation is analogous to that observed in ref. 23 for $g^{(2)}(\tau)$ for the light from a single ion, which arose from micromotion of the ion in the radio-frequency trap.

Here, $U(\mathbf{r}) = U_0 \sin^2(2\pi x/\lambda_{C_2})\exp(-2\rho^2/w^2_{C_2})$ is the FORT potential, which gives rise to an anharmonic ladder of vibrational states with energies $\{E_m\}$. Here $m = 0$ to $m_{\mathrm{max}} = 99$ correspond to the bound states in the axial dimension for radial coordinate $\rho \equiv \sqrt{y^2 + z^2} = 0$. The anharmonicity leads to the observed offset $f_0 < \nu_0$ due to the distribution of energies for axial motion in the FORT well. Indeed, the frequency $\nu_{\mathrm{min}} = (E_{m_{\mathrm{max}}} - E_{m_{\mathrm{max}}-1})/h$ at the top of the well is approximately half that at the bottom of the well, $\nu_0 = (E_1 - E_0)/h$. By comparing the measured distribution of frequencies exhibited by $\tilde{g}(f)$ with the calculated axial frequencies $\{\nu_m\}$, we estimate that those atoms from which data was obtained are trapped in the lowest-lying axial states $m \lesssim 10$, which corresponds to a maximum energy $E/k_B \approx 250\,\mu\mathrm{K}$. This energy estimate is consistent with other measurements of $g^{(2)}_{yz}(\tau)$ that we have made, as well as the Fourier transform of the record of the transmitted intensity and the transmission spectra of ref. 21.

We have demonstrated photon blockade for the transmission of an optical cavity strongly coupled to a single trapped atom[4–9,12,13]. The observed nonclassical photon statistics for the transmitted field result from strong nonlinear interactions at the single-photon level, in analogy with the phenomena of Coulomb blockade for electron transport[1–3]. Extensions of our work include operation in a pulsed mode, as was analysed in ref. 5, thereby realizing a source for single photons 'on demand'[22]. As we improve the effectiveness of our cooling procedure, we should be able to explore the dependence of $g^{(2)}_{yz}(\tau)$ on probe detuning, $\omega_p - \omega_0$, as well as to move to higher levels of excitation to increase the intracavity photon number towards unity and the output flux towards the maximum value $\lesssim \kappa$ for subpoissonian photons.

METHODS

Cavity and detection parameters. The physical length of the cavity used in this work is 42.2 μm and the finesse is 4.3×10^5. The cavity length is independently stabilized such that a TEM_{00} longitudinal mode at λ_{C_1} is resonant with the free-space atomic transition at λ_A and another TEM_{00} mode at λ_{C_2} is resonant at λ_F. At the cavity centre $x = 0$, the mode waists $w_{C_{1,2}} = \{23.4, 24.5\}$ μm at $\lambda_{C_{1,2}} = \{852.4, 935.6\}$ nm.

The TEM_{00} longitudinal mode for the FORT is driven by a linearly polarized input field ε_{FORT}, resulting in nearly equal a.c. Stark shifts for Zeeman states in the $6S_{1/2},\ F=3,4$ manifold. At an antinode of the field, the peak value of the trapping potential for these states is $U_0/h=-43\,\mathrm{MHz}$ for all our measurements. Zeeman states of the $6P_{3/2},\ F'=5'$ manifold experience a similar trapping potential, but with a weak dependence on m_F' (ref. 18).

Stress-induced birefringence in the cavity mirrors leads to a mode splitting $\Delta\omega_{C_1}/2\pi=4.4\pm0.2\,\mathrm{MHz}$ of the two cavity modes $l_{y,z}$ with orthogonal linear polarizations $(\hat{y},\hat{z})$. ε_{FORT} is linearly polarized and aligned along $\hat{z}$, the higher-frequency mode.

The efficiency for photon escape from the cavity, limited by losses inherent to the mirror substrates, is $\alpha_{\mathcal{E}2}=0.6\pm0.1$. The propagation efficiency from M_2 to detectors (D_1, D_2) is $\alpha_P=0.41\pm0.03$, with each detector then receiving half of the photons. The avalanche photodiodes (D_1, D_2) have quantum efficiencies $\alpha_D=0.49\pm0.05$.

Photon statistics. The transmission spectrum $T(\omega_p)$ is proportional to the ratio of photon flux $\langle\varepsilon_t^{\dagger}\varepsilon_t\rangle$ transmitted by M_2 to the flux $|\varepsilon_p|^2$ incident upon M_1, and normalized such that a cavity without an atom has a resonant transmission of unity, i.e. $T(\omega_p=\omega_{C_1})=1$. For a field with intensity operator $\hat{I}(t), g^{(2)}(\tau)\equiv\langle:\hat{I}(t)\hat{I}(t+\tau):\rangle/\langle:\hat{I}(t):\rangle\langle:\hat{I}(t+\tau):\rangle$, where the colons denote time and normal ordering (ref. 17). $g^{(2)}_{yz}(\tau)$, displayed in Fig. 3a and shown with a 6-ns resolution, has been corrected for background counts due to detector dark counts and scattered light from the repumping beam. Without this correction, $g^{(2)}_{yz}(0)\simeq(0.18\pm0.10)$ is directly derived from the recorded counts.

Received 26 March; accepted 5 May 2005.

1. Fulton, T. A. & Dolan, G. J. Observation of single-electron charging effects in small tunnel junctions. *Phys. Rev. Lett.* **59,** 109–112 (1987).
2. Kastner, M. A. The single-electron transistor. *Rev. Mod. Phys.* **64,** 849–858 (1992).
3. Likharev, K. K. Single-electron devices and their applications. *Proc. IEEE* **87,** 606–632 (1999).
4. Tian, L. & Carmichael, H. J. Quantum trajectory simulations of two-state behavior in an optical cavity containing one atom. *Phys. Rev. A* **46,** R6801 (1992).
5. Imamoğlu, A., Schmidt, H., Woods, G. & Deutsch, M. Strongly interacting photons in a nonlinear cavity. *Phys. Rev. Lett.* **79,** 1467–1470 (1997).
6. Grangier, P., Walls, D. F. & Gheri, K. M. Comment on "Strongly interacting photons in a nonlinear cavity". *Phys. Rev. Lett.* **81,** 2833 (1998).
7. Werner, M. J. & Imamoğlu, A. Photon-photon interactions in cavity electromagnetically induced transparency. *Phys. Rev. A* **61,** 011801 (1999).
8. Rebić, S., Tan, S. M., Parkins, A. S. & Walls, D. F. Large Kerr nonlinearity with a single atom. *J. Opt. B* **1,** 490–495 (1999).
9. Rebić, S., Parkins, A. S. & Tan, S. M. Polariton analysis of a four-level atom strongly coupled to a cavity mode. *Phys. Rev. A* **65,** 043806 (2002); Photon statistics of a single-atom intracavity system involving electromagnetically induced transparency. *Phys. Rev. A* **65,** 063804 (2002).
10. Kim, J., Bensen, O., Kan, H. & Yamamoto, Y. A single-photon turnstile device. *Nature* **397,** 500–503 (1999).
11. Smolyaninov, I. I., Zayats, A. V., Gungor, A. & Davis, C. C. Single-photon tunneling via localized surface plasmons. *Phys. Rev. Lett.* **88,** 187402 (2002).
12. Brecha, R. J., Rice, P. R. & Xiao, M. N two-level atoms in a driven optical cavity: quantum dynamics of forward photon scattering for weak incident fields. *Phys. Rev. A* **59,** 2392–2417 (1999).
13. Hood, C. J. *Real-time Measurement and Trapping of Single Atoms by Single Photons*. Section 6.2. PhD dissertation, California Institute of Technology (2000).
14. Kimble, H. J. Strong interactions of single atoms and photons in cavity QED. *Phys. Scr.* **T76,** 127–138 (1998).
15. Jaynes, E. T. & Cummings, F. W. Comparison of quantum and semiclassical radiation theories with application to the beam maser. *Proc. IEEE* **51,** 89–109 (1963).
16. Kimble, H. J., Dagenais, M. & Mandel, L. Photon antibunching in resonance fluorescence. *Phys. Rev. Lett.* **39,** 691–695 (1977).
17. Mandel, L. & Wolf, E. *Optical Coherence and Quantum Optics* (Cambridge Univ. Press, Cambridge, 1995).
18. McKeever, J. *et al.* State-insensitive cooling and trapping of single atoms in an optical cavity. *Phys. Rev. Lett.* **90,** 133602 (2003).
19. Carmichael, H. J., Brecha, R. J. & Rice, P. R. Quantum interference and collapse of the wavefunction in cavity QED. *Opt. Commun.* **82,** 73–79 (1991).
20. Carmichael, H. J. Photon antibunching and squeezing for a single atom in a resonant cavity. *Phys. Rev. Lett.* **55,** 2790–2793 (1985).
21. Boca, A. *et al.* Observation of the vacuum Rabi spectrum for one trapped atom. *Phys. Rev. Lett.* **93,** 233603 (2004).
22. McKeever, J. *et al.* Deterministic generation of single photons from one atom trapped in a cavity. *Science* **303,** 1992–1994 (2004).
23. Diedrich, F. & Walther, H. Nonclassical radiation of a single stored ion. *Phys. Rev. Lett.* **58,** 203–260 (1987).

Supplementary Information is linked to the online version of the paper at www.nature.com/nature.

Acknowledgements We gratefully acknowledge the contributions of J. McKeever and C. J. Hood. This research is supported by the National Science Foundation, by the Caltech MURI Center for Quantum Networks, and by the Advanced Research and Development Activity (ARDA).

Author Information Reprints and permissions information is available at npg.nature.com/reprintsandpermissions. The authors declare no competing financial interests. Correspondence and requests for materials should be addressed to H.J.K. (hjkimble@caltech.edu).